Persistent Homology Reveals Loop Hierarchy and Recirculation Risk in Underground Mine Ventilation Networks

Shadrack Nuamah[1], Abhishek Choudhury[1], Atish Mitra[2], and Ian Pfeffer[1]

[1]Department of Mining Engineering, Montana Technological University,
snuamah@mtech.edu, AChoudhury@mtech.edu, ipfeffer@mtech.edu
[2]Department of Mathematical Sciences, Montana Technological University,
amitra@mtech.edu

Abstract

Underground mine ventilation sustains safe working conditions by supplying fresh air, diluting contaminants, and controlling heat and humidity throughout active workings. Because air moves through a connected system of shafts, drifts, and raises, the ventilation problem is inherently one of network flow-and in large mines, that network can grow complex enough that standard simulation tools, while numerically reliable, leave engineers with little guidance on which circuits matter most, which redundancy is structurally meaningful, and where recirculation risk is concentrated. We address this gap by developing a physics-guided topological workflow that layers three complementary analyses: a physical graph filtration on real airway adjacency, an adjacency-preserving flag complex companion, and resistance-geodesic Vietoris-Rips persistent homology. The physical graph filtration preserves all existing airway circuits, the flag complex applies a stricter structural test through clique completion, and the resistance-geodesic branch recasts the network as an operational metric space in which loop persistence is governed by cumulative airway resistance. Together, these three branches distinguish circuits that physically exist in the mine from those that remain topologically persistent once resistance is taken into account. The framework was applied to Montana Tech's Underground Mine Education Center (UMEC) under two operating conditions—natural ventilation and main-fan-assisted flow with two auxiliary fans off—using field-calibrated Ventsim® models as the network basis. Under natural ventilation, two persistent H1 loops emerged, with the southern circuit nearly an order of magnitude stronger than the upper loop; under fan assistance, the upper loop disappeared entirely, leaving only the southern circuit. The disappearance of the upper loop is physically coherent-the exhaust fan draws air outward through that branch, preventing it from sustaining a closed resistance-informed circuit. The southern loop's persistence across both operating states identifies it as the network's most structurally stable redundancy candidate and the strongest target for recirculation-focused engineering attention. These results demonstrate that persistent homology can complement conventional ventilation analysis by providing a grounded, resistance-informed method for ranking loop structures according to recirculation potential.

Keywords:
mine ventilation, persistent homology, topological data analysis, graph filtration, Vietoris-Rips complex, recirculation

1 Introduction

Underground mine ventilation is the principal engineered system responsible for maintaining safe and workable subsurface conditions. It distributes fresh air through active workings, removes hazardous

contaminants such as diesel particulate matter and noxious gases, and helps control the thermal and humidity conditions that influence worker safety, equipment performance, and overall underground mine operations [9, 13]. In practice, the ventilation problem is inherently network-based: air moves through a connected system of shafts, drifts, raises, stopes, and regulators, while fans and natural pressure differences drive flow through airways with differing resistances [9, 13]. For this reason, mine ventilation has long been modeled and analyzed as a graph-constrained flow system, with commercial and research tools such as Ventsim® DESIGN and VNet/VnetPC providing predictive solutions for quantities, pressures, and scenario testing [17, 19].

Despite the maturity of ventilation network analysis, several interpretive challenges remain in large and geometrically complex mines. Engineers may be able to solve the network numerically and obtain stable airflow distributions, yet still face difficulty in identifying which loops matter most, which alternative routes represent meaningful redundancy, and which parts of the network are most susceptible to recirculation-prone behavior under changing operating conditions [9, 13, 19, 17]. In practice, not every geometric cycle in a mine layout is equally important. Some loops may be weak, short-lived, or operationally irrelevant, whereas others may indicate structurally important circulation circuits capable of supporting redistributed flow or persistent redundancy. A method that can rank such structures across scale, while remaining grounded in engineering interpretation, would therefore be valuable.

Topological Data Analysis (TDA), and persistent homology in particular, offers one possible framework for addressing this challenge. Persistent homology summarizes how connected components and loop-like structures appear and disappear as a filtration parameter varies, providing a multi-scale description of network topology [1, 5, 7, 14]. This is attractive in ventilation analysis because redundancy, circuit formation, and alternative routing are all fundamentally related to network structure. However, the direct application of persistent homology to ventilation graphs requires careful modeling choices. Persistent homology is computed on an all-pairs resistance-geodesic distance matrix derived from the ventilation graph in the operational branch of the analysis. That representation remains useful because it captures the resistance-informed operational geometry of the network, but it also raises an important interpretive consideration: shortest-path proximity in a derived metric space does not necessarily preserve the distinction between physically existing airways and pairwise relations implied indirectly through multi-edge paths.

The framework presented in this paper addresses this issue by decomposing the analysis into two complementary layers. The first layer is a physical-topology baseline constructed directly from the original ventilation adjacency and implemented primarily as a graph filtration on real airways. This branch preserves physically existing closed circuits, including triangular airway loops that may be relevant to local recirculation or leakage interpretation. An adjacency-preserving weighted flag complex is then used as a stricter companion analysis on the same physical graph, so that broader loop-supporting structure can be distinguished from local cycles that disappear under clique completion. The second layer is a resistance-informed topology constructed from resistance-geodesic distances, which recasts the ventilation network as an operational metric space governed by cumulative resistance. Under this interpretation, loops emerging in the resistance-conditioned shadow graph are not considered as meaningful in isolation, but rather as operationally relevant when supported by corresponding structures in the physical-topology baseline, thereby avoiding a purely abstract metric interpretation and instead grounding these features in circuits that are physically realizable within the mine network.

Accordingly, this paper develops a physics-guided topological workflow for underground ventilation networks that combines adjacency-preserving graph topology, resistance-geodesic persistent homology, and graph-cycle localization. The framework is intended not to replace conventional ventilation analysis, but to complement it by providing a structured way to identify, rank, and

interpret persistent loop structures that may matter for redundancy, alternative routing, and recirculation potential.

1.1 Related Work

Ventilation network analysis is traditionally formulated through conservation of mass at junctions and conservation of energy around circuits, with pressure losses governed by the square-law resistance relationship commonly expressed through the Atkinson equation [9, 13]. Classical circuit-balancing methods such as Hardy Cross and related iterative techniques laid the foundation for solving nonlinear network flows [4], while modern ventilation practice relies heavily on simulation environments that implement these principles at full-network scale and support calibration, scenario analysis, and optimization [17, 19]. More recent work has extended this tradition through model reconciliation, CFD-assisted calibration, and optimization of fans and regulators using mathematical programming and metaheuristics [8, 11, 12, 16, 21].

In parallel, TDA has emerged as a robust mathematical framework for studying structure in complex data. Persistent homology tracks topological features across a filtration and summarizes them using persistence diagrams, barcodes, Betti curves, and related descriptors [1, 5, 7, 14]. Applications to weighted networks have shown that persistent homology can reveal influential cycles and higher-order structural organization that are not easily captured by standard graph metrics alone [15]. These developments motivate its use in mine ventilation, where loop structure, redundancy, and the possibility of redistributed or recirculating flow are central engineering concerns. Nevertheless, the published literature on persistent-homology-based analysis of mine ventilation networks remains limited, especially with respect to workflows that are both mathematically careful and directly interpretable by ventilation engineers.

1.2 Our Contributions

This work makes four contributions.

First, it introduces an adjacency-preserving physical-topology baseline for mine ventilation networks, implemented as an edge-weighted graph filtration on real airways so that physically existing closed circuits, including triangular recirculation candidates, are preserved explicitly.

Second, it formulates an adjacency-preserving weighted flag complex companion in which physical airway edges are weighted by recorded airway length when available and by Euclidean node-to-node distance only as a fallback, thereby providing a stricter structural test beyond simple graph closure.

Third, it develops a resistance-geodesic Vietoris-Rips branch that recasts the ventilation network as an operational metric space capturing resistance-defined connectivity, redundancy, and loop persistence.

Fourth, it establishes a comparative interpretation framework in which graph-filtration loops, flag complex loops, and resistance-geodesic persistent features are evaluated jointly, allowing physically existing circuits, broader structurally supported loops, and resistance-defined redundancy signatures to be distinguished more defensibly in recirculation-related interpretation.

2 Methods

2.1 Conceptual Foundations and Case-study Context

Persistent homology builds a multiscale topological description from simplices and nested filtrations [5, 1, 7, 14]. Figure 1 summarizes the geometric building blocks of persistent homology and their

barcode representation, while Figure 2 shows the important distinction between a graph and its associated clique complex. This distinction matters in the present study because clique completion fills triangle-supported closures and therefore provides a stricter test of whether an observed airway circuit remains an H_1-relevant loop.

The case study for this work is the Underground Mining Education Center (UMEC) at Montana Tech. Figure 3 shows the plan view of the study area, including the current design, UMEC workings, and historic workings. Figure 4 shows the calibrated Ventsim® model with the selected survey locations used in the pressure-quantity (P-Q) comparison, and Figure 5 shows the computational ventilation network representation colored by airflow. These figures establish the physical and computational context for the topological analyses reported in the subsequent sections.

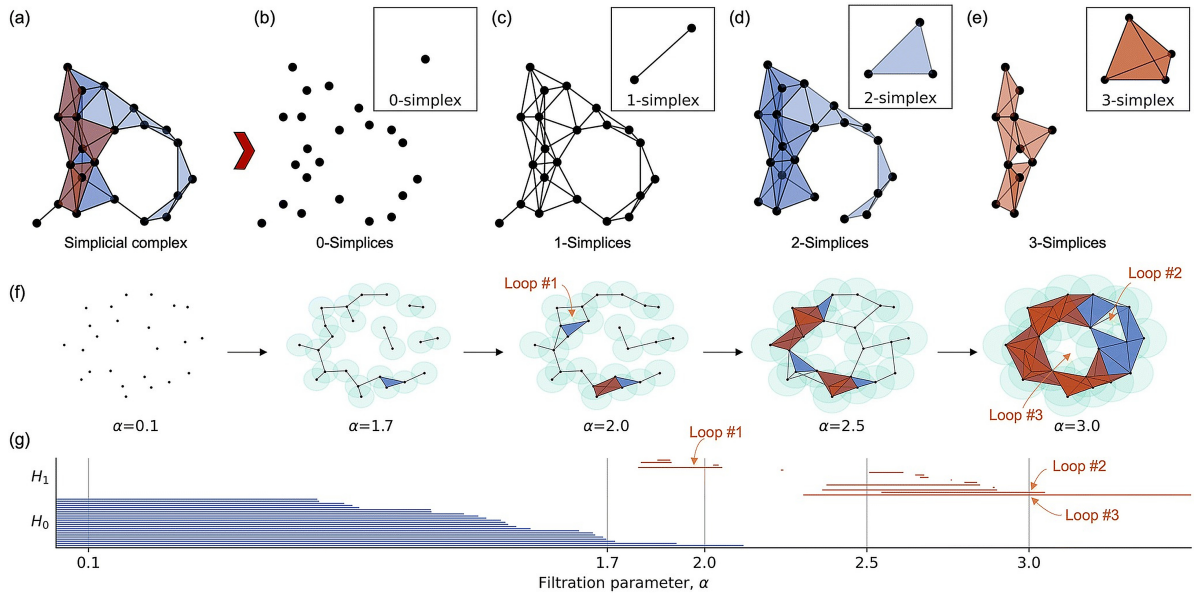

Figure 1: Illustration of Persistent Homology Concepts, Showing Simplex Dimensions, a Nested Filtration, and the Corresponding Barcode Representation of H_0 and H_1 Features [2].

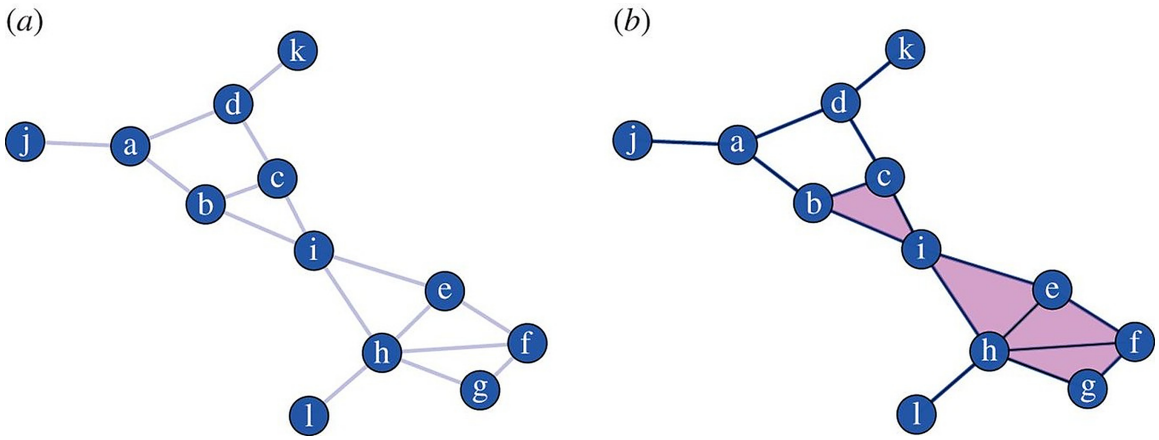

Figure 2: (a) Original Graph Representation; (b) Clique Complex Derived from the Graph [15].

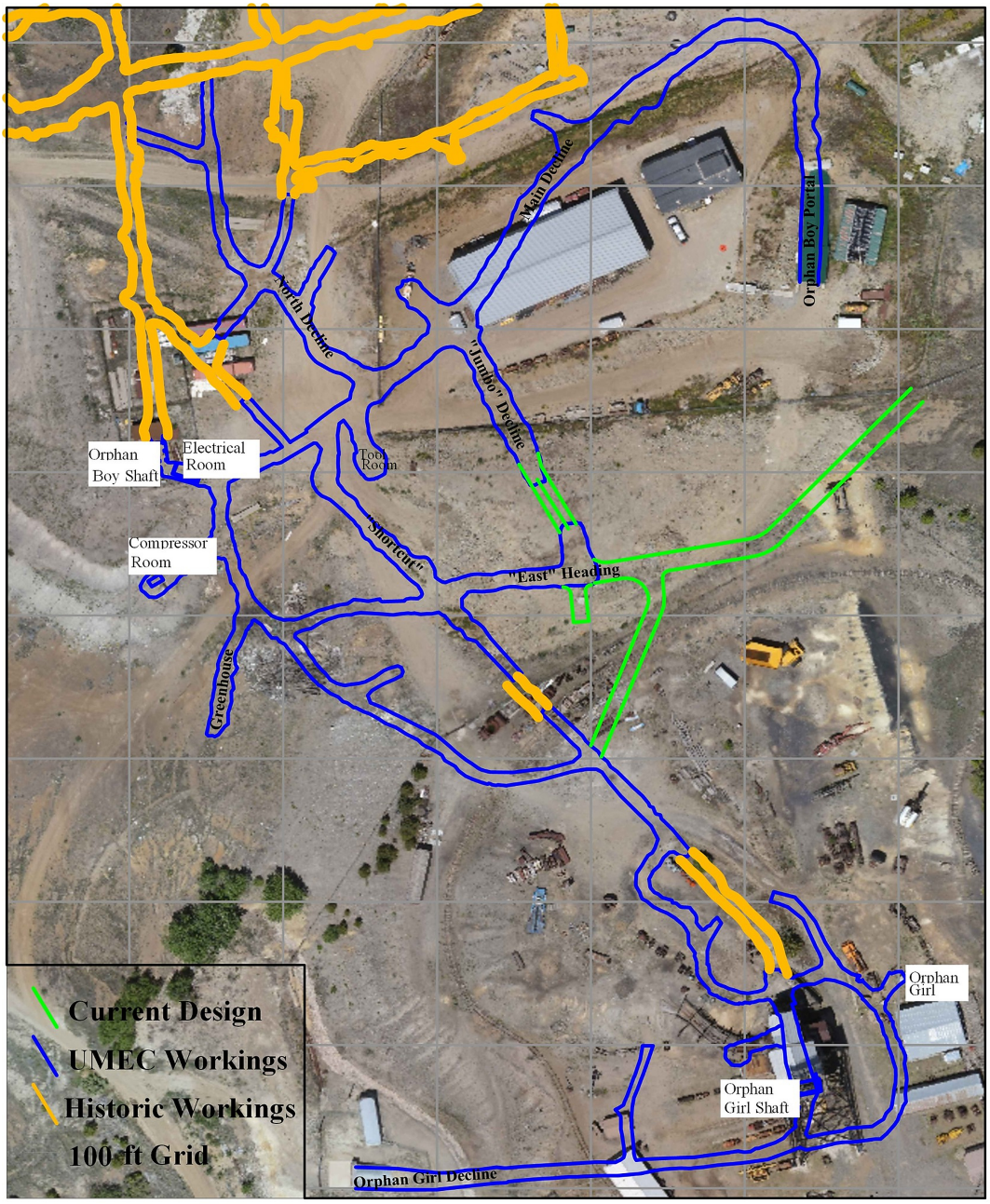

Figure 3: Plan View of the Underground Mining Education Center (UMEC) Study Area.

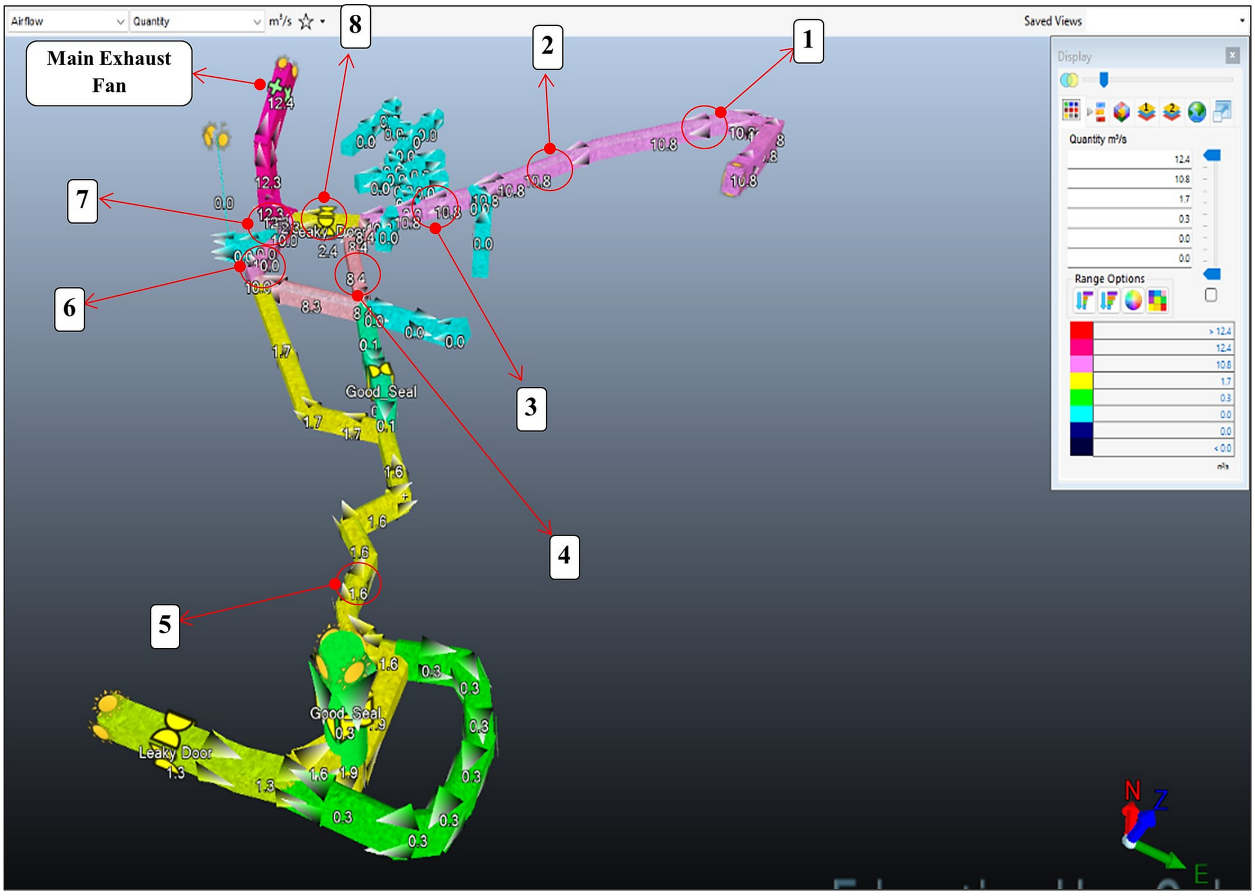

Figure 4: Ventsim Model of UMEC, Showing the Selected Survey Locations Labeled and Indexed According to the Corresponding Tables and Main Fan Location.

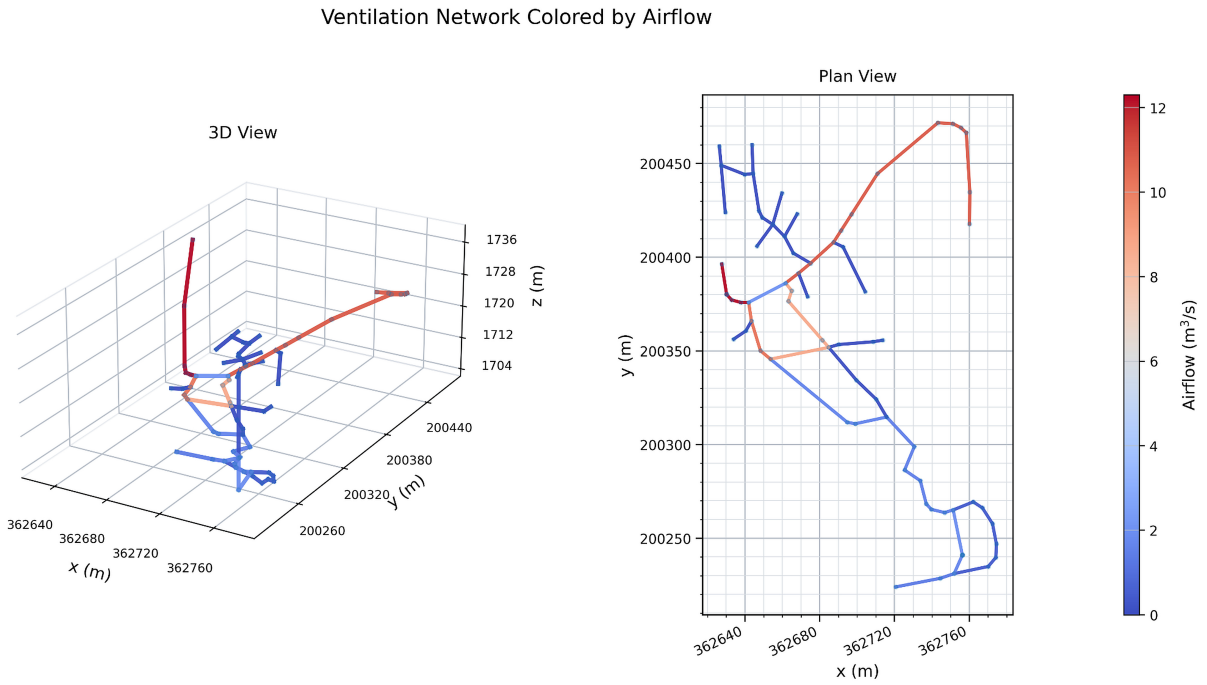

Figure 5: Spatial Network of the UMEC Ventilation Network Colored by Airflow, Generated from the Computational Workflow Used for Ventilation Network Analysis, Showing the 3D View (Left) and Plan View (Right).

The proposed workflow represents a ventilation model as a weighted graph extracted from standard network software or survey-based mine-network descriptions [3, 9, 13, 19]. Nodes correspond to junctions or endpoints with spatial coordinates, while edges correspond to physically existing airways characterized by attributes such as length, airflow quantity, and resistance [3, 9, 13]. In the present study, the Underground Mine Education Center (UMEC) at Montana Technological University serves as the case-study network. The implementation is carried out in Python using NumPy and Pandas for data handling, giotto-tda for persistent-homology computation, NetworkX for graph procedures, and Matplotlib for visualization [18]. In this study, persistent homology is computed through a physical graph-filtration branch on the original ventilation adjacency, an adjacency-preserving flag complex companion on the same physical graph, and a resistance-geodesic metric branch derived from the same network.

2.2 Mathematical Preliminaries

2.2.1 Network Model and Notation

The underground ventilation layout is represented as a weighted graph $G = (V, E)$, where each vertex $v \in V$ denotes a junction or endpoint (e.g., split, intersection, raise collar), and each edge $e = (i, j) \in E$ denotes a physically existing airway connecting nodes i and j [3, 9, 13]. Each airway carries attributes such as geometric length L_e (m), airflow quantity Q_e (m^3/s), and resistance R_e ($\mathrm{N{\cdot}s^2/m^8}$) [9, 13]. A standard quadratic resistance model (Atkinson-type square-law) relates pressure loss to airflow [9, 13]:

$$\Delta H_e = R_e \, Q_e^2, \tag{1}$$

where ΔH_e is the pressure drop (head loss) across airway e [9, 13]. In the framework developed here, two edge-weight interpretations are retained. For the physical-topology baseline, the preferred geometric weight is the recorded airway segment length,

$$w_{\text{phys}}(e) = L_e, \tag{2}$$

with Euclidean node-to-node distance used only as a fallback when explicit airway lengths are unavailable,

$$w_{\text{phys}}(e) = \|\mathbf{x}_i - \mathbf{x}_j\|_2. \tag{3}$$

For the operational branch,

$$w_R(e) = R_e, \tag{4}$$

for the resistance-informed analysis. This distinction is central to the interpretation of the resulting persistent features.

2.2.2 Physical-layout Baseline using a Graph Filtration

To establish which loop-supporting structure is physically present in the mine, the original ventilation adjacency is preserved and filtered directly. Let

$$E_\tau^{\text{phys}} = \{(i,j) \in E : w_{\text{phys}}(i,j) \leq \tau\} \tag{5}$$

be the set of real airways whose geometric weight does not exceed threshold τ. These edges define a thresholded subgraph

$$G_\tau^{\text{phys}} = (V, E_\tau^{\text{phys}}). \tag{6}$$

The primary physical topology filtration is taken to be the corresponding 1-dimensional cell complex,

$$X_\tau^{\text{phys}} = V \cup E_\tau^{\text{phys}}, \tag{7}$$

with no 2-simplices or higher-dimensional simplices added [1, 5, 7]. Under this construction, only physically existing airways can generate edges in the filtration, and an H_1 feature corresponds to a closed circuit supported by actual mine adjacency. In particular, triangular 3-cycles formed by real airways remain detectable as physically existing loop candidates rather than being filled immediately by clique completion.

2.2.3 Adjacency-preserving Flag complex Companion

To distinguish broader loop-supporting structure from purely local graph closure, the same thresholded physical graph is also analyzed through a weighted flag complex companion:

$$\text{Flag}_{\text{phys}}(\tau) = \text{Cl}(G_\tau^{\text{phys}}), \tag{8}$$

where every complete subgraph in G_τ^{phys} is promoted to a simplex [5, 7, 15]. This companion construction preserves the original mine adjacency but applies clique completion, $Cl(\cdot)$ as a stricter structural test. Consequently, triangular 3-cycles are filled immediately in this branch, while larger loops survive only when they are not explained by immediate local triangulation.

2.2.4 Resistance-geodesic Distance and the Operational Metric Space

To characterize resistance-informed connectivity and redundancy, the same ventilation graph is also analyzed using resistance as the edge weight [3, 9, 13]. For any path $p = (v_0, v_1, \ldots, v_m)$ from $i = v_0$ to $j = v_m$, define its resistance length as

$$L_R(p) = \sum_{k=0}^{m-1} w_R(v_k, v_{k+1}) = \sum_{e \in p} R_e. \tag{9}$$

The resistance-geodesic distance between nodes i and j is then

$$d_R(i, j) = \min_{p:\, i \to j} \sum_{e \in p} R_e. \tag{10}$$

Collecting these all-pairs distances yields the matrix

$$D_R = [d_R(i, j)]_{i,j \in V}, \tag{11}$$

which defines an operational metric space on the node set [3, 6, 18, 20]. This representation is valuable because low-resistance routes become close in the induced metric, but it must be interpreted differently from the physical adjacency graph because two non-adjacent nodes may become close through a multi-edge path.

2.2.5 Minimum Spanning Tree and Kruskal's Algorithm

A spanning tree T connects all vertices without cycles [3]. The minimum spanning tree (MST) is the spanning tree minimizing total edge weight [3, 10]:

$$T^* = \arg \min_{T \text{ spanning tree}} \sum_{e \in T} w_R(e). \tag{12}$$

With $w_R(e) = R_e$, the MST provides a resistance-efficient connectivity backbone for the network [3, 9, 13]. Kruskal's algorithm constructs T^* by sorting edges by increasing R_e and adding edges that connect distinct components [3, 10]. Any edge that would connect two already connected vertices becomes a closing edge and defines a fundamental cycle with the unique tree path between its endpoints. This logic is retained for representative loop localization after persistence computation.

2.2.6 All-pairs Shortest Paths and Computation of D_R

An all-pairs shortest-path solution is required to compute D_R on the resistance-weighted graph [3, 6, 20]. In dense settings this may be obtained by Floyd-Warshall, while repeated Dijkstra solves are appropriate for sparse graphs [6, 20]. In the implementation used here, a graph-geodesic operator is employed to compute the full resistance-geodesic matrix directly from the weighted adjacency [18]. The resulting matrix is validated to ensure finiteness, non-negativity, and zero diagonal entries before persistent homology is applied.

2.2.7 Related Filtrations Used in This Study

This study employs three related filtrations, each with a distinct interpretive role.

The physical graph filtration is given by the 1-dimensional complex X_τ^{phys}, which describes how the adjacency-preserving mine structure grows with increasing geometric threshold while preserving

all physically existing closed circuits, including triangles [5, 7, 15]. This branch addresses the question: *Which closed circuits are physically present in the mine layout?*

The companion physical flag-complex filtration is given by $\mathrm{Flag}_{\mathrm{phys}}(\tau)$, which applies clique completion to the same thresholded physical graph and therefore acts as a stricter test of loop-supporting structure beyond immediate local triangulation [5, 7, 15]. This branch addresses the question: *Which physical loops remain structurally meaningful after clique completion?*

The resistance-informed filtration is defined by the Vietoris-Rips complex on the resistance-geodesic matrix:

$$\mathrm{VR}_R(\tau) = \{\sigma \subseteq V \mid d_R(u,v) \leq \tau \text{ for all } u,v \in \sigma\}. \tag{13}$$

Vertices are always present, edges appear when pairwise resistance-geodesic distances fall below the threshold, and higher-dimensional simplices appear when all pairwise distances within a vertex set satisfy the same condition [5, 7, 14]. Unlike the physical graph and flag-complex branches, this filtration is constructed from the derived metric space rather than the original graph adjacency. This branch addresses the question: *Which physical loops remain topologically persistent when airway resistance is incorporated into the operational geometry of the network?*

These three branches are required because no single topological construction can simultaneously preserve every physically existing airway circuit and also provide a stricter ventilation-relevant ranking of loop significance. The physical graph branch retains all closed airway circuits, including triangular loops that may still matter for local recirculation, leakage, or airflow redundancy. The flag-complex companion then tests whether a candidate loop remains meaningful once immediate clique-supported closure is removed. The resistance-geodesic Vietoris-Rips branch finally evaluates whether those structures remain prominent after airway resistance is introduced into the filtration. Used together, the three branches provide a physically grounded and progressively stricter interpretation of loop significance.

Table 1: Summary of the Complementary Roles of the Three Topological Branches Used in This Study.

Method	**Role**
Graph filtration	Identifies physically existing airway circuits, including triangular recirculation candidates.
Flag complex	Applies a stricter structural test by filling clique-supported triangles and retaining only loops that remain significant beyond immediate local closure.
Resistance-geodesic Vietoris-Rips analysis	Evaluates loops using resistance-weighted network distance and ranks them by persistence, helping distinguish the circuits with higher recirculation potential from weaker local closures.

Together, the three methods are complementary: the graph filtration identifies which circuits physically exist, the adjacency-preserving flag complex tests whether they remain meaningful after local clique closure, and the resistance-geodesic Vietoris-Rips analysis determines which of those circuits or loops remain most persistent once ventilation resistance is taken into account.

2.2.8 Filtration Scale, Computational Thresholds, and Reporting Scope

The filtration parameter τ has different meanings in the physical and operational analyses. In the physical graph and companion flag complex branches, τ is a geometric threshold on real airways

and therefore reflects the growth of the actual mine graph under weighted adjacency. In the resistance-geodesic analysis, τ represents resistance-induced shortest-path distance and therefore reflects accessibility in the operational resistance geometry of the network. No fixed uniform filtration increment was prescribed in the implementation. Instead, the persistence computations are evaluated at the critical values induced by the edge weights or distance entries that define the corresponding filtration [5, 7, 18].

The figures reported in this paper are drawn primarily from the resistance-geodesic branch of the workflow for the UMEC case study, while the physical graph filtration establishes which circuits physically exist and the companion physical flag complex branch provides the stricter structural reference used in interpretation.

Several additional numerical thresholds were used in the implementation, but these served only as safeguards for numerical stability or visualization. For example, a very small positive constant was used to replace non-positive resistance values, and separate display thresholds were used for plotting zoomed persistence diagrams and persistence images. These settings did not alter the underlying filtration definitions; rather, they improved the robustness and readability of the computational outputs.

2.2.9 Homology Groups, Betti Numbers, and Comparative Interpretation

Homology summarizes topology by dimension. In this study, the analysis focuses on H_0, which counts connected components, and H_1, which captures independent loop-like features [1, 5, 7]. At threshold τ, the Betti number

$$\beta_k(\tau) = \operatorname{rank} H_k(\mathcal{K}(\tau)) \tag{14}$$

counts the number of k-dimensional features in the active complex $\mathcal{K}(\tau)$ [1, 5]. Persistent homology records the birth and death of each feature across the filtration, and a feature born at $\tau = b$ and dying at $\tau = d$ has persistence, Π

$$\Pi = d - b. \tag{15}$$

In the present framework, persistence is interpreted comparatively rather than absolutely. Features that appear in the physical graph filtration are treated as physically existing circuits in the mine layout. If those same features are also supported by the companion physical flag complex analysis, they are interpreted as broader structural loops that are not explained merely by local triangular closure. Features that are additionally recovered in the resistance-geodesic Vietoris-Rips analysis are treated as the strongest candidates for circuits that are both physically present and operationally significant. Features that appear only in the resistance-geodesic analysis are interpreted more cautiously as resistance-defined redundancy signatures.

2.2.10 Loop Localization and Engineering Interpretation

To support engineering interpretation, representative graph cycles are extracted from the original ventilation graph using a Kruskal sweep and fundamental-cycle logic [3, 10]. For a persistence point (b, d) in the resistance-geodesic analysis, the midpoint filtration scale is defined as a representative resistance threshold:

$$\tau = \frac{b + d}{2}. \tag{16}$$

Each candidate loop is represented by a closing edge $e_{\text{close}} = (i, j)$ together with an alternative path connecting the same endpoints in the spanning tree. Let $P_T(i, j)$ denote the unique path between i and j in the spanning tree T. The resistance of the closing edge is

$$R_{\text{direct}} = w_R(e_{\text{close}}) = R_{e_{\text{close}}}, \tag{17}$$

the cumulative resistance of the alternative tree path is

$$R_{\text{path}} = \sum_{e \in P_T(i,j)} w_R(e) = \sum_{e \in P_T(i,j)} R_e, \tag{18}$$

and the total cycle resistance summary is

$$R_{\text{cycle}} = R_{\text{direct}} + R_{\text{path}}. \tag{19}$$

For the resistance-geodesic formulation, matched cycles are treated as representative physical candidates used to interpret persistent H_1 signatures rather than as exact one-to-one topological equivalents. When a localized cycle is also supported by the physical graph filtration, it is confirmed as a physically existing circuit; when it is additionally supported by the companion physical flag complex branch, confidence is stronger that the feature reflects broader loop-supporting structure rather than only local triangular closure.

2.2.11 When a Candidate Cycle Becomes a Persistent Loop

Not every graph-theoretic cycle in the ventilation network corresponds to a persistent topological loop. A candidate cycle first arises at the graph level when a closing edge connects two nodes that are already joined by an alternative path, thereby forming a fundamental cycle [3, 10]. At this stage, the structure is only a potential loop in the combinatorial sense.

In the physical graph filtration, a loop is born when the final real edge needed to close an adjacency-supported circuit enters the thresholded graph. Because no 2-simplices are added in this branch, a closed circuit, including a triangular 3-cycle, remains an H_1-relevant feature for the remainder of the filtration and is therefore reported primarily by its birth scale and geometry. In the companion physical flag complex branch, the same candidate survives as an H_1 loop only if it is not immediately filled by clique completion; triangular 3-cycles are therefore removed in this stricter structural test. In the resistance-geodesic branch, a candidate cycle becomes an H_1 loop only when it appears as an independent one-dimensional hole in the Vietoris-Rips filtration constructed from the resistance-geodesic distance matrix [5, 7, 14]. This occurs at its birth scale b, where the relevant simplices are present but the cycle has not yet been filled in by additional higher-order simplex connections. It becomes a persistent loop when that hole survives over a nonzero filtration interval $[b, d)$, where d denotes the death scale.

Loop significance is therefore governed not merely by the existence of a closed path, but by its stability across the selected filtration. In the present framework, the strongest interpretation is assigned to loops that are present in the physical graph branch and remain meaningful in the stricter flag-complex and resistance-geodesic branches.

2.2.12 Assumptions, Scope, and Validity

This analysis assumes the ventilation network can be treated as a static weighted graph where airway resistances R_e are sufficiently stable for comparative structural analysis [9, 13]. The resistance-weighted distance $d_R(i, j)$ focuses on connectivity and redundancy and therefore treats the network as undirected for topological characterization, even though operational airflows have direction and may vary with fans, regulators, and production conditions [9, 13]. The physical baseline likewise abstracts the network to its undirected structural adjacency. Consequently, the results primarily describe structural redundancy and resistance-based accessibility rather than time-varying flow behavior under changing control settings [5, 9, 13, 14]. Despite these simplifications, geometric layout and airway resistance remain physically meaningful descriptors for identifying robust alternative pathways,

bottlenecks, and critical redundancy substructures that complement conventional ventilation network analysis [9, 13].

2.2.13 Computational Workflow

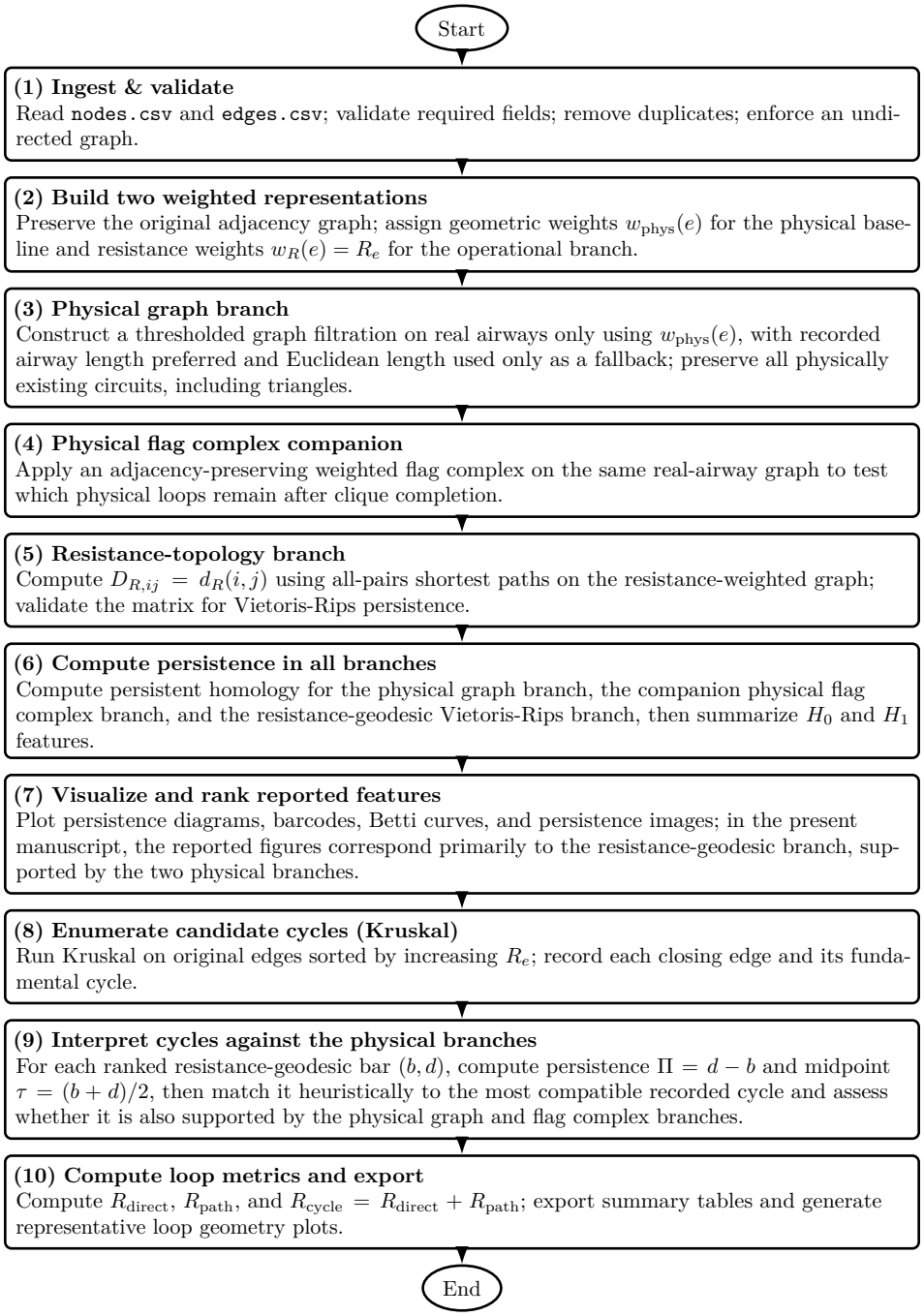

Figure 6: Updated workflow for ventilation-network topology. The procedure separates a physical graph-filtration baseline that preserves real airway circuits, an adjacency-preserving physical flag complex companion, and a resistance-geodesic Vietoris-Rips analysis, then uses graph-cycle localization to interpret reported H_1 features.

3 Results and Discussion

Two common operating conditions for the UMEC network were evaluated: natural ventilation and a fan-assisted state with the main fan on and two auxiliary fans off. In both cases, the Ventsim® model was first calibrated against field P-Q survey measurements and then interrogated using the three-branch topological workflow described in the Methods section.

3.1 Ventilation Model Calibration

3.1.1 Natural Ventilation

Table 2 summarizes the P-Q survey data for the natural-ventilation condition. Measured quantities are low throughout the network, with the highest measured values observed at SMD 07 (1.3 m^3/s) and Post Bend/Tool Room (1.2 m^3/s), while the lowest values occur at SMD 15 and the section between the Compressor Room and the Electrical Room (0.1 m^3/s). These values are consistent with a weakly driven system in which airflow is distributed through the available workings but remains limited in magnitude. The model reproduces the measured values closely, with only minor deviations at the lowest-flow locations.

Table 2: Pressure-Quantity (P-Q) Survey Results for UMEC Under the Condition: Natural Ventilation, Showing Measured and Modeled Airflow Quantities at Selected Locations.

#	Location	Pressure ($in.H_2O$)	Dry Bulb t_d (°F)	Wet Bulb t_w (°F)	Avg. Vel. (fpm)	Area (ft^2)	Quantity (Measured) (kcfm)	Quantity (Measured) (m^3/s)	Quantity (Model) (kcfm)	Quantity (Model) (m^3/s)
1	Post Bend	26.77	42	41	27.0	97.4	2.6	1.2	2.6	1.2
2	SMD 07	26.85	42	41	32.0	83.1	2.7	1.3	2.6	1.2
3	Tool Room	26.88	44	42	29.0	87.0	2.5	1.2	2.6	1.2
4	Shortcut (Before Ballroom and Fan)	26.87	43	41	34.5	63.0	2.2	1.0	2.1	1.0
5	1L07	26.85	45	44	24.0	74.4	1.8	0.8	1.6	0.8
6	SMD 15	26.85	49	46	4.0	53.5	0.2	0.1	0.4	0.2
7	Between Compressor Room and Electrical Room	26.86	49	46	2.0	65.9	0.1	0.1	0.3	0.1
8	Concrete (Behind "Air Door")	26.86	46	44	6.5	64.8	0.4	0.2	0.5	0.2

Figure 7 confirms the fidelity of the natural-ventilation model. The calibration points lie close to the 1:1 line and produce $R^2 = 0.9925$, indicating that the simulated quantities are sufficiently consistent with the field measurements to support topological interpretation on the calibrated network [19, 21, 12].

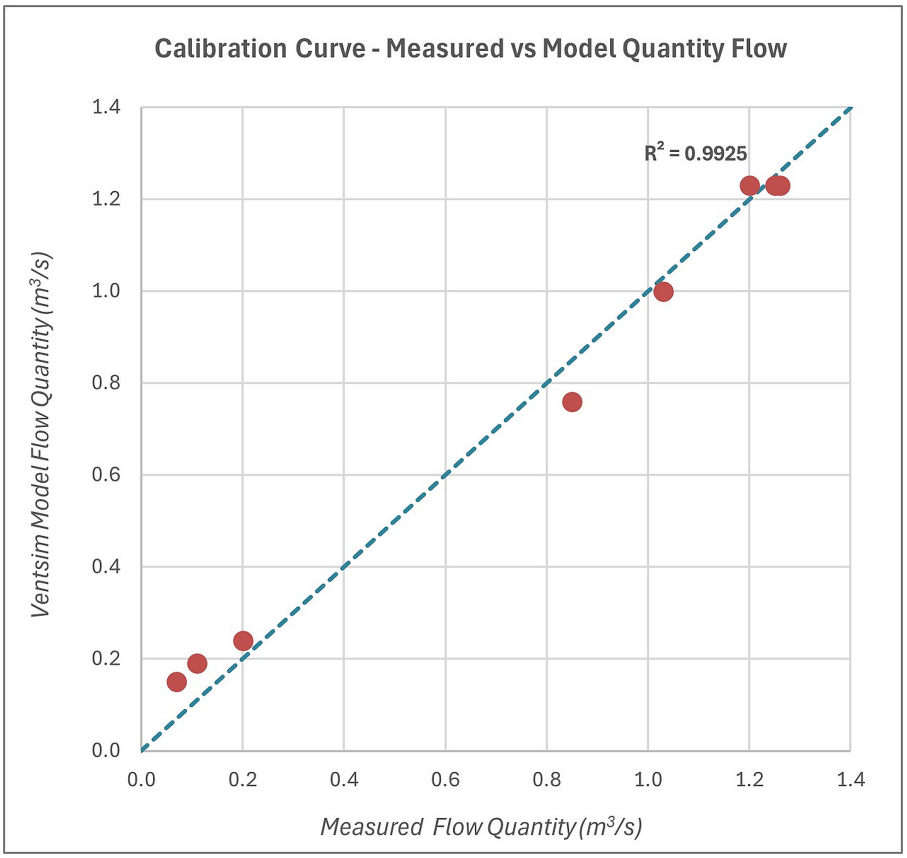

Figure 7: Calibration Curve for the UMEC P-Q Survey Under the Condition: Natural Ventilation, Comparing Measured Flow Quantity with Ventsim Modeled Flow Quantity and Demonstrating a Strong Correlation Between the Two ($R^2 = 0.9925$).

3.1.2 Main Fan on and Two Auxiliary Fans off

Table 3 summarizes the P-Q survey results for the main-fan-assisted condition. Relative to natural ventilation, airflow magnitudes increase substantially across the network. The major monitored locations near the upper workings carry measured quantities of approximately 10.7–10.8 m^3/s, while the central shortcut carries 8.3 m^3/s and the lower-flow zones still carry between 1.4 and 2.5 m^3/s. This indicates that the main fan imposes a much clearer dominant routing structure on the network than the natural-ventilation case.

Table 3: Pressure-Quantity (P-Q) Survey Results for UMEC Under the Condition: Main Fan On and Two Auxiliary Fans Off, Showing Measured and Modeled Airflow Quantities at Selected Locations.

#	Location	Pressure ($in.H_2O$)	Dry Bulb t_d (°F)	Wet Bulb t_w (°F)	Avg. Vel. (fpm)	Area (ft^2)	Quantity (Measured) (kcfm)	Quantity (Measured) (m^3/s)	Quantity (Model) (kcfm)	Quantity (Model) (m^3/s)
1	Post Bend	26.60	30	29	235.0	97.4	22.9	10.8	22.9	10.8
2	SMD 07	26.62	33	31	273.0	83.1	22.7	10.7	22.9	10.8
3	Tool Room	26.66	38	35	261.5	87.0	22.7	10.7	22.9	10.8
4	Shortcut (Before Ballroom and Fan)	26.66	38	36	280.0	63.0	17.7	8.3	17.8	8.4
5	1L07	26.68	45	45	38.5	74.4	2.9	1.4	3.3	1.6
6	SMD 15	26.66	42	41	397.5	53.5	21.3	10.0	21.2	10.0
7	Between Compressor Room and Electrical Room	26.67	42	41	318.5	65.9	21.0	9.9	21.1	10.0
8	Concrete (Behind "Air Door")	26.66	40	38	80.5	64.8	5.2	2.5	5.1	2.4

Figure 8 shows an even tighter agreement between field measurements and model predictions than the natural-ventilation case, with $R^2 = 0.9996$. The calibrated Ventsim® model therefore provides a reliable basis for comparing how the topological signatures change between the weakly driven and strongly driven operating conditions [19, 21, 12].

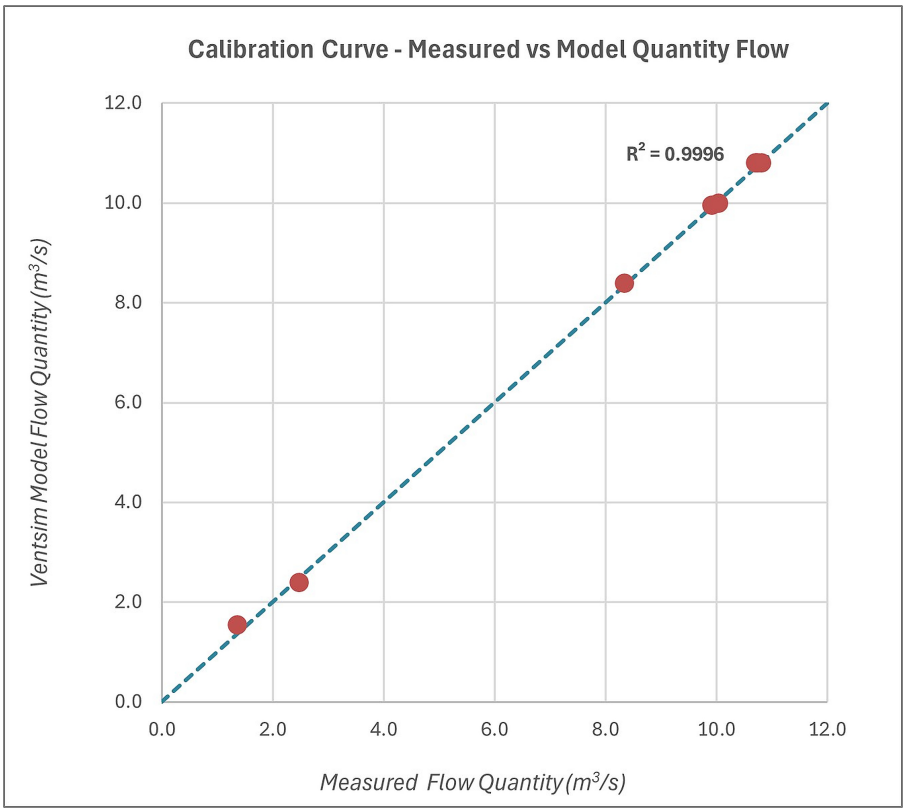

Figure 8: Calibration Curve for the UMEC P-Q Survey Under the Condition: Main Fan On and Two Auxiliary Fans Off, Comparing Measured Flow Quantity with Ventsim Modeled Flow Quantity and Demonstrating a Strong Correlation Between the Two ($R^2 = 0.9996$).

3.2 Topological Results for Natural Ventilation Condition

The natural-ventilation state reveals the richest loop structure in the study. Figure 9 compares the physically existing closed circuits identified through adjacency-preserving flag complex matching with the structurally significant loops retained by the resistance-geodesic Vietoris-Rips analysis. In the physical branch, three closed circuits are visible in the matched geometry. After resistance weighting and persistent-homology ranking, only two loops remain as nontrivial H_1 features in the resistance-informed branch.

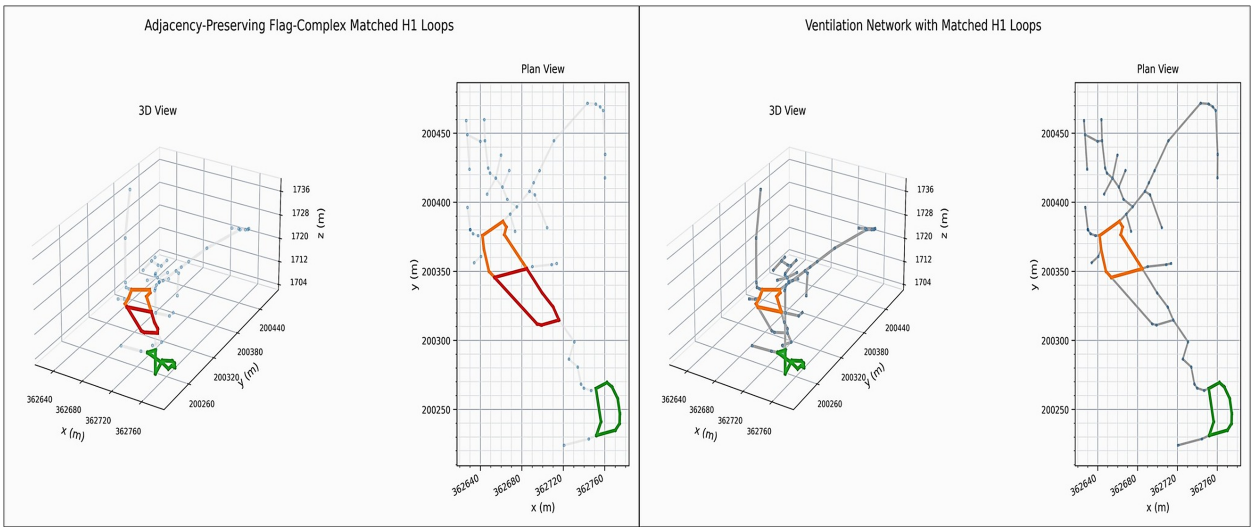

Figure 9: Highest-Persistence H1 Loops for UMEC Under the Condition: Natural Ventilation, Showing the Closed Circuits Present in the Mine Geometry Through Adjacency-Preserving Flag Complex Matching (Left) and the Corresponding Structurally Significant Loops Distinguished by the Resistance-Geodesic Vietoris-Rips Analysis for Recirculation-Related Interpretation (Right).

The persistence diagrams in Figure 10 show that the natural-ventilation condition contains two persistent H_1 loops. The smaller orange loop has $\Pi = 0.00143$, whereas the southern green loop has $\Pi = 0.01743$, making it the dominant resistance-informed loop feature in this state. The barcode and Betti-curve results in Figure 11 are consistent with this interpretation: β_1 rises to two over a limited filtration interval and then returns to zero as the loop-supporting structure is filled in at larger thresholds. From an engineering standpoint, this means that natural ventilation preserves more than one nontrivial redundancy circuit when the network is interpreted through the resistance-geodesic metric. The southern loop is the strongest candidate for higher recirculation potential, while the orange loop remains present but substantially weaker.

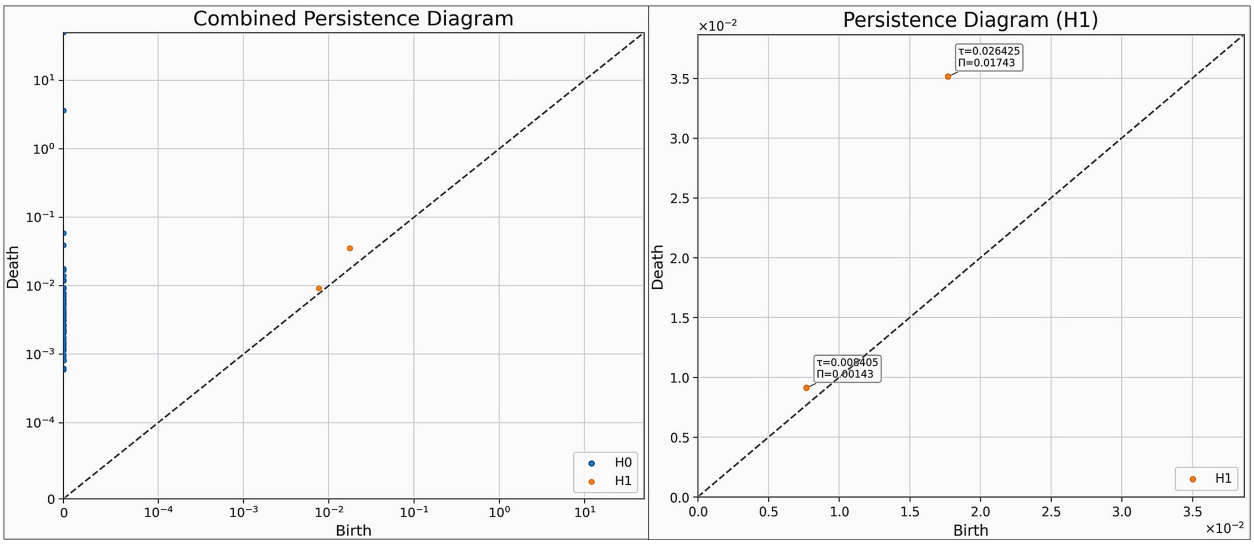

Figure 10: Persistence Diagrams for UMEC Under the Condition: Natural Ventilation, Showing the Combined Persistence Diagram for H0 and H1 Features (Left) and the H1 Persistence Diagram Identifying Two Persistent Loops (Right), Corresponding to the Orange Loop and Green Loop in Figure 9, with Persistence Values of $\Pi = 0.00143$ and $\Pi = 0.01743$, Respectively.

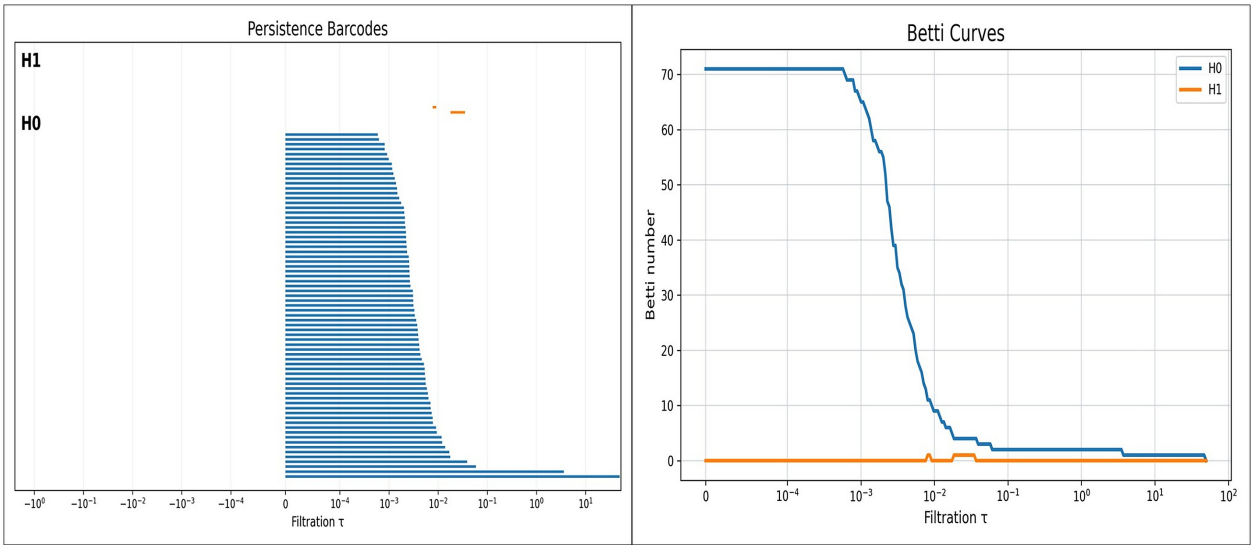

Figure 11: Persistence Barcode and Betti Curve Results for UMEC Under the Condition: Natural Ventilation, Showing the Persistence Barcodes for H0 and H1 Features (Left) and the Corresponding Betti Curves Across the Filtration Range (Right).

3.3 Topological Results for the Main Fan Assisted Condition

The main-fan-assisted case exhibits a simpler resistance-informed topology. Because the main fan operates as an exhaust fan, it pulls air out of the upper workings and imposes a stronger outward draw near the fan location [9, 13]. Mechanistically, this makes the loop closest to the main fan less able to reclose as a sustained circulation circuit, because air is preferentially extracted rather than allowed to circulate locally around that upper branch. Figure 12 shows that although multiple circuits are still present in the physical mine geometry, only one loop remains as a persistent H_1 feature once the network is filtered through the resistance-geodesic Vietoris-Rips construction.

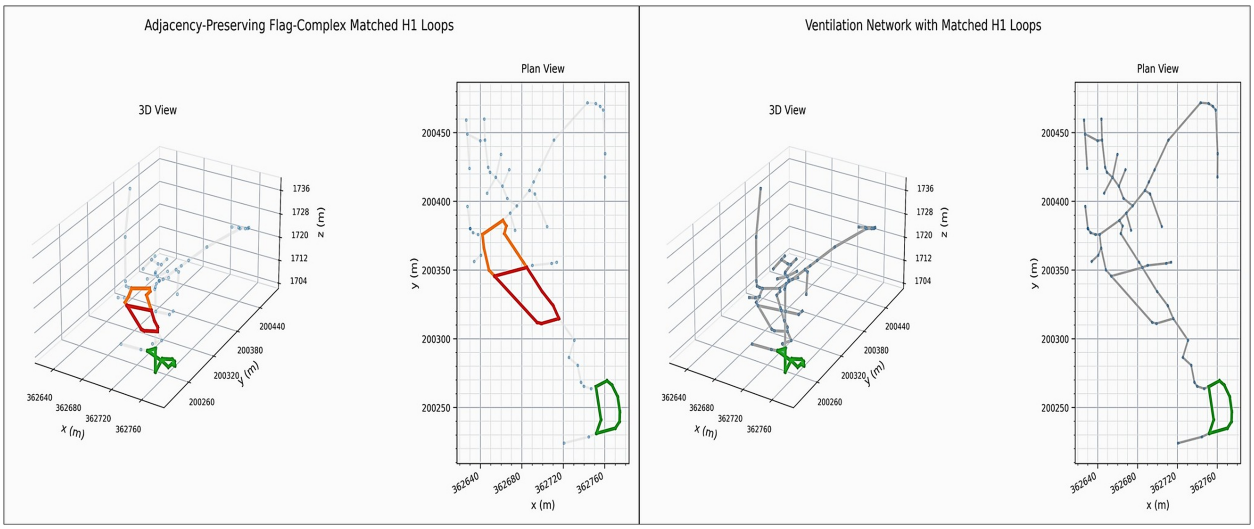

Figure 12: Highest-Persistence H1 Loop for UMEC Under the Condition: Main Fan On and Two Auxiliary Fans Off, Showing the Closed Circuit Present in the Mine Geometry Through Adjacency-Preserving Flag Complex Matching (Left) and the Corresponding Structurally Significant Loop Distinguished by the Resistance-Geodesic Vietoris-Rips Analysis for Recirculation-Related Interpretation (Right).

Figure 13 shows a single nontrivial H_1 feature with $\Pi = 0.00143$, corresponding to the green loop. The loop closest to the main fan, which is still visible in the physical branch, no longer survives as a persistent resistance-informed feature. This behavior is consistent with the exhaust role of the main fan: by pulling air outward through the upper branch, the fan weakens the ability of that local circuit to reclose as a sustained resistance-informed loop [9, 13]. The barcode and Betti-curve results in Figure 14 confirm this simplification, with β_1 reaching one only briefly before returning to zero. This indicates that the main fan reorganizes the resistance-weighted topology into a more strongly hierarchical flow structure. The physically existing loops are not removed from the mine geometry, but only one of them retains sufficient persistence to stand out as a higher-recirculation-potential candidate in the operational metric space.

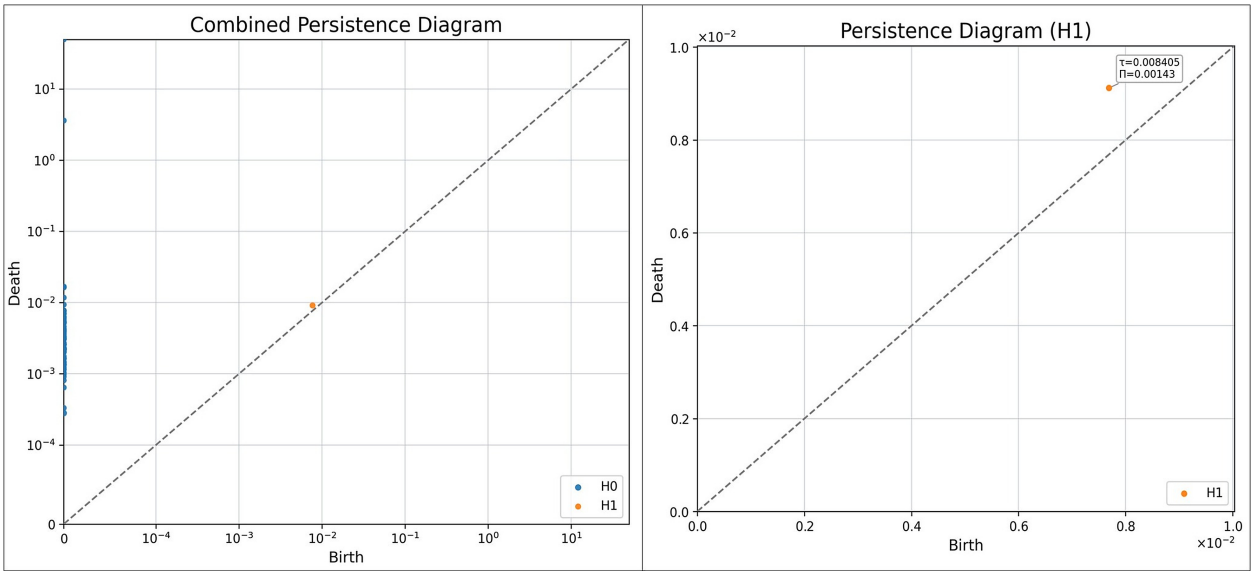

Figure 13: Persistence Diagrams for UMEC Under the Condition: Main Fan On and Two Auxiliary Fans Off, Showing the Combined Persistence Diagram for H0 and H1 Features (Left) and the H1 Persistence Diagram Identifying One Persistent Loop (Right), Corresponding to the Green Loop in Figure 12, with a Persistence Value of $\Pi = 0.00143$.

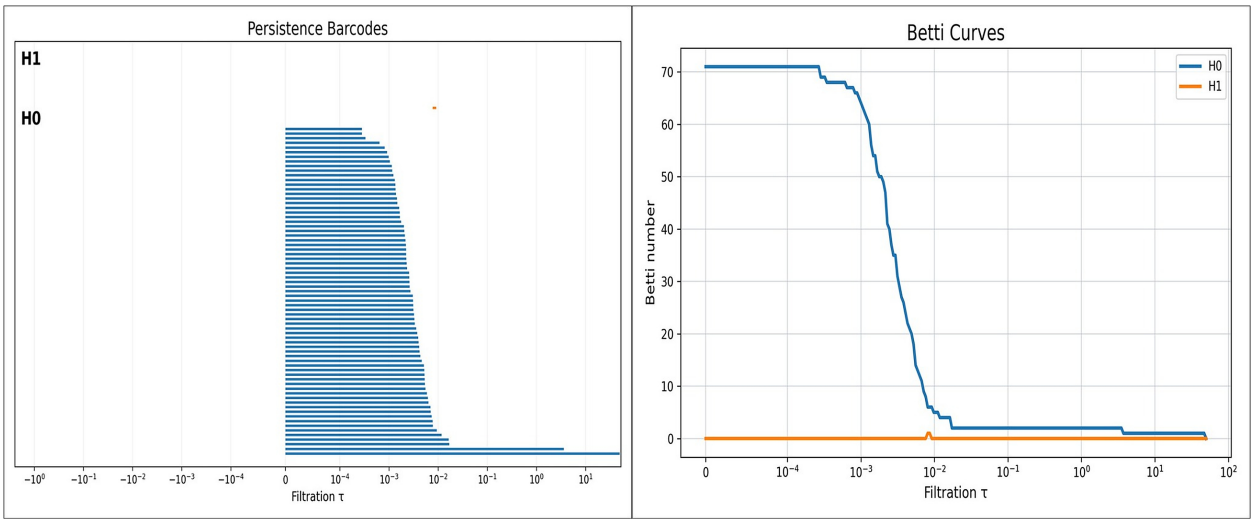

Figure 14: Persistence Barcode and Betti Curve Results for UMEC Under the Condition: Main Fan On and Two Auxiliary Fans Off, Showing the Persistence Barcodes for H0 and H1 Features (Left) and the Corresponding Betti Curves Across the Filtration Range (Right).

3.4 Comparative Interpretation Across the Two Common Operating Conditions

The side-by-side comparison of the two calibrated operating states shows the value of separating physical adjacency from resistance-informed persistence. The physical mine geometry continues to contain multiple closed circuits under both operating conditions. However, the resistance-geodesic branch ranks these circuits differently once resistance-weighted shortest-path structure is taken into account.

Under natural ventilation, two persistent H_1 loops are retained, with the southern green loop clearly dominant ($\Pi = 0.01743$) and the orange loop remaining as a weaker secondary feature ($\Pi = 0.00143$). Under the main-fan-assisted state, only the southern green loop remains persistent, and its persistence is reduced to $\Pi = 0.00143$. This comparison suggests that the natural-ventilation state preserves a more distributed redundancy structure in the resistance-informed topology, whereas the exhaust action of the main fan concentrates the operational flow structure and suppresses the persistence of the loop nearest the fan branch [9, 13].

These results also clarify why the three-branch interpretation is necessary. The physical graph filtration establishes that the circuits are actually present in the mine layout. The adjacency-preserving flag complex provides a stricter structural reference against immediate local closure. The resistance-geodesic Vietoris-Rips branch then identifies which of those physical circuits remain topologically persistent once airway resistance is incorporated. In practical ventilation terms, the southern loop emerges as the most condition-invariant circuit in the network and therefore the strongest candidate for closer recirculation-focused engineering scrutiny. At the same time, the topological workflow should not be interpreted as direct proof of recirculation; rather, it provides a mathematically grounded screening method for identifying loop structures with higher recirculation potential that merit further ventilation analysis, scenario testing, or tracer-based validation.

4 Conclusions

This paper presents a physics-guided topological workflow for underground mine ventilation analysis that separates physically existing airway circuits from resistance-informed operational topology. The framework combines a physical graph filtration, an adjacency-preserving flag complex companion, and a resistance-geodesic Vietoris-Rips analysis so that loop structures can be interpreted progressively rather than through a single abstract topological representation.

The UMEC case study shows that this separation is useful in practice. First, the calibrated Ventsim® models were strongly supported by field P-Q survey data, with $R^2 = 0.9925$ for the natural-ventilation condition and $R^2 = 0.9996$ for the condition with the main fan on and two auxiliary fans off. Second, the resistance-geodesic branch revealed a clear difference in loop persistence between operating states. Natural ventilation produced two persistent H_1 loops with persistence values of $\Pi = 0.00143$ and $\Pi = 0.01743$, whereas the main-fan-assisted state produced only one persistent H_1 loop with $\Pi = 0.00143$. The southern circuit represented by the green loop remained present in both states and therefore emerged as the most condition-invariant structurally significant loop in the network, while the upper loop nearest the main fan collapsed in the fan-assisted case because the exhaust fan pulled air out of that branch and prevented the loop from remaining closed and persistent [9, 13].

These findings show that the proposed workflow does more than enumerate graph cycles. It distinguishes between circuits that merely exist in the mine geometry and circuits that remain topologically persistent after resistance-weighted operational structure is taken into account. In ventilation-engineering terms, this provides a grounded way to rank loop structures according to higher recirculation potential while avoiding the stronger claim that persistence alone proves

recirculation.

The study therefore demonstrates that persistent homology can complement, rather than replace, conventional ventilation-network analysis. By combining calibrated ventilation modeling with physical and resistance-informed topology, the workflow provides a practical screening tool for identifying structurally important airway circuits, prioritizing locations for deeper engineering inspection, and supporting future work on recirculation-focused diagnostics, scenario testing, and ventilation optimization [9, 13, 19, 21].

References

[1] Carlsson, G. (2009). Topology and data. Bulletin of the American Mathematical Society, 46(2), 255-308. https://doi.org/10.1090/S0273-0979-09-01249-X

[2] Chen, D., Chen, C.L., & Wei, G. W. (2025). Category-specific topological learning of metal-organic frameworks. *Journal of Materials Chemistry A*, 13, 9292-9303. https://doi.org/10.1039/D4TA08877H

[3] Cormen, T. H., Leiserson, C. E., Rivest, R. L., & Stein, C. (2009). Introduction to Algorithms (3rd ed.). MIT Press and McGraw-Hill.

[4] Cross, H. (1936). Analysis of flow in networks of conduits or conductors. Bulletin 286, Engineering Experiment Station, University of Illinois.

[5] Edelsbrunner, H., & Harer, J. (2010). Computational Topology: An Introduction. American Mathematical Society. https://doi.org/10.1090/mbk/069

[6] Floyd, R. W. (1962). Algorithm 97: Shortest path. Communications of the ACM, 5(6), 345. https://doi.org/10.1145/367766.368168

[7] Ghrist, R. (2008). Barcodes: The persistent topology of data. Bulletin of the American Mathematical Society, 45(1), 61-75. https://doi.org/10.1090/S0273-0979-07-01191-3

[8] Goldberg, D. E. (1989). Genetic Algorithms in Search, Optimization and Machine Learning. Addison-Wesley.

[9] Hartman, H. L., Mutmansky, J. M., Ramani, R. V., & Wang, Y. J. (1997). Mine Ventilation and Air Conditioning (3rd ed.). John Wiley & Sons.

[10] Kruskal, J. B. (1956). On the shortest spanning subtree of a graph and the traveling salesman problem. Proceedings of the American Mathematical Society, 7(1), 48-50. https://doi.org/10.1090/S0002-9939-1956-0078686-7

[11] Lewis, A. E., & Hugo, A. (2000). A combined method for the analysis of mine ventilation networks. Journal of the Southern African Institute of Mining and Metallurgy, 100(6), 371-373.

[12] Maleki, S., Sotoudeh, F., & Sereshki, F. (2018). Application of VENTSIM 3D and mathematical programming to optimize underground mine ventilation network: A case study. Journal of Mining and Environment, 9(3), 741-752. https://doi.org/10.22044/jme.2018.6793.1503

[13] McPherson, M. J. (1993). Subsurface Ventilation and Environmental Engineering. Springer. https://doi.org/10.1007/978-94-011-1550-6

[14] Otter, N., Porter, M. A., Tillmann, U., Grindrod, P., & Harrington, H. A. (2017). A roadmap for the computation of persistent homology. EPJ Data Science, 6, 17. https://doi.org/10.1140/epjds/s13688-017-0109-5

[15] Petri, G., Expert, P., Turkheimer, F., Carhart-Harris, R., Nutt, D., Hellyer, P. J., & Vaccarino, F. (2014). Homological scaffolds of brain functional networks. Journal of the Royal Society Interface, 11(101), 20140873. https://doi.org/10.1098/rsif.2014.0873

[16] Shang, W., & Jia, J. (2025). Theoretical knowledge enhanced genetic algorithm for mine ventilation system optimization considering main fan adjustment. Complex & Intelligent Systems, 11, Article 16. https://doi.org/10.1007/s40747-024-01619-5

[17] SRK Consulting. (2019). VNet User Manual and Tutorial. SRK Consulting (VNet/VnetPC).

[18] Tauzin, G., Lupo, U., Tunstall, L., Burella Pérez, J., Caorsi, M., Medina-Mardones, A. M., Dassatti, A., & Hess, K. (2021). giotto-tda: A topological data analysis toolkit for machine learning and data exploration. Journal of Machine Learning Research, 22(39), 1-6.

[19] Ventsim. (2024). Ventsim DESIGN User Manual. Ventsim Software. (Accessed 2026-02).

[20] Warshall, S. (1962). A theorem on Boolean matrices. Journal of the ACM, 9(1), 11-12. https://doi.org/10.1145/321105.321107

[21] Xu, G., Huang, J., Nie, B., Chalmers, D., & Yang, Z. (2018). Calibration of Mine Ventilation Network Models Using the Non-Linear Optimization Algorithm. Energies, 11(1), 31. https://doi.org/10.3390/en11010031